Temperature, Sensitivity, and Frequency Response of AlN/GaN Heterostructure Micro-Hall Effect Sensor

Satish Shetty, Savannah R. Eisner, Ayesha Hassan, Anand Lalwani, Dinesh Baral, Yuriy I. Mazur, Debbie G. Senesky, *Senior Member, IEEE*, H. O. H. Churchill, Zhong Chen, *Member, IEEE*, H. Alan Mantooth, *Fellow, IEEE*, and Gregory J. Salamo

***Abstract*— We report for the first time on an aluminum nitride/gallium nitride (AlN/GaN) heterostructure as a microscale Hall effect sensor for current sensing applications in extreme environments. The AlN/GaN devices demonstrated high signal linearity as a function of the magnetic field across a temperature range from −193 °C to 407 °C. The measured room temperature (RT) supply voltage-related sensitivity (S_{svrs}) and supply current-related sensitivity (S_{scrs}) are 0.055 T^{-1} and 32 $VA^{-1}T^{-1}$, respectively. The supply power-related sensitivity (S_{sprs}) is 1.4 $VW^{-1}T^{-1}$ above 40-mW input bias, which is higher than that of the $Al_{0.2}Ga_{0.8}N$/GaN device. The designed AlN/GaN micro-Hall sensor is further determined to have a lower power consumption and higher temperature sensitivity than equivalent $Al_{0.2}Ga_{0.8}N$/GaN Hall devices. When operated in an ac bias mode, the rise time of the Hall sensor was found to be 102 ns, corresponding to a frequency bandwidth of 9.8 MHz. We also observed a phase shift between an applied magnetic field and the Hall sensor signal, which can potentially be helpful to monitor ac line currents.**

***Index Terms*— Aluminum nitride/gallium nitride (AlN/GaN), bandwidth, Hall effect sensor, high-electron-mobility transistor (HEMT), high frequency, offset voltage, two-dimensional electron gas (2DEG).**

Manuscript received 29 December 2023; revised 29 February 2024; accepted 25 March 2024. Date of publication 8 April 2024; date of current version 24 April 2024. This work was supported by the Army (ARL); Toward a SiC CMOS Process for Advanced Integration, under Grant W911NF-21-2-0231. The work of H. O. H. Churchill was supported by the MonArk NSF Quantum Foundry through the National Science Foundation Q-AMASE-i Program under NSF Award DMR-1906383. The review of this article was arranged by Editor G. Crupi. *(Corresponding author: Satish Shetty.)*

Satish Shetty, Dinesh Baral, Yuriy I. Mazur, H. O. H. Churchill, and Gregory J. Salamo are with the Institute for Nanoscience and Engineering, University of Arkansas, Fayetteville, AR 72701 USA (e-mail: satishshettymn@gmail.com; dbaral@uark.edu; ymazur@uark.edu; hchurch@uark.edu; salamo@uark.edu).

Savannah R. Eisner is with the Department of Electrical Engineering, Columbia University, New York, NY 10027 USA (e-mail: savannah.eisner@columbia.edu).

Ayesha Hassan, Zhong Chen, and H. Alan Mantooth are with the Department of Electrical Engineering, University of Arkansas, Fayetteville, AR 72701 USA (e-mail: ah111@uark.edu, chenz@uark.edu, mantooth@uark.edu).

Anand Lalwani and Debbie G. Senesky are with the Department of Aeronautics and Astronautics, Stanford University, Stanford, CA 94305 USA (e-mail: anandl@stanford.edu; dsenesky@stanford.edu).

Color versions of one or more figures in this article are available at https://doi.org/10.1109/TED.2024.3382643.

Digital Object Identifier 10.1109/TED.2024.3382643

I. Introduction

HALL effect sensors are an excellent diagnostic tool that are utilized to protect electronic devices by monitoring current levels and fluctuations at the system level. Applications to monitor the current in engines, motors, and power modules, with rapid response, require Hall effect sensors able to operate from dc to high frequencies above 20 MHz [1], [2] and at high temperatures exceeding ∼800 °C. The available state-of-the-art Hall effect sensors based on silicon, GaAs, and InAs are currently limited to temperatures ≤150 °C and frequencies around 200 kHz [3], [4], [5], [6]. Meanwhile, wide bandgap semiconductor devices are demonstrated to operate at temperatures as high as 1000 °C [7] and frequencies higher than 100 MHz [7], [8], making them an excellent choice of material for Hall sensors that function at high temperatures, high frequencies, and within harsh environments.

For this research, an aluminum nitride/gallium nitride (AlN/GaN) two-dimensional electron gas (2DEG) was selected as a Hall sensor due to a high breakdown field (∼3.3 × 10^6 V/cm), mobility (∼1800 cm^2/Vs), and electron saturation velocity (∼2.5 × 10^7 cm/s), as well as a low dielectric constant (∼5.3) [6], [7], [8]. Moreover, aluminum nitride possesses a strong spontaneous polarization that enables the fabrication of AlN/GaN heterostructures characterized by excellent electrical properties. The high sheet density 2DEG, high mobility, and subsequent low sheet resistance supported by the AlN/GaN heterostructure are important to realize Hall sensor devices with high switching speeds, low insertion losses [3], [4], [5], [6], and low *RC* time constants.

Taking advantage of these properties, we report on AlN/GaN micro-Hall effect sensors capable of monitoring circuit currents operating at high temperature and high frequency. The fabricated AlN/GaN micro-Hall effect sensors exhibit high signal linearity under a wide range of current (∼0.2–12 mA) and voltage (∼0.5–10 V) biases for a significant range of applied magnetic field (50 mT–0.25 T) amplitudes. The AlN/GaN micro-Hall sensor also exhibits low power consumption and higher temperature sensitivity as well as excellent temperature stability from −193 °C to 407 °C. The sheet resistance of the AlN/GaN Hall sensor linearly increases with temperature over a range of 30 °C–380 °C and has a temperature coefficient of ∼9200 ppm/°C, which enables

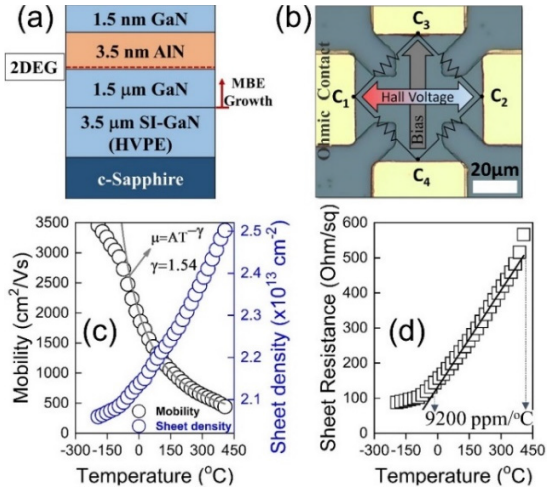

Fig. 1. (a) Cross-sectional diagram of AlN/GaN heterostructure, (b) optical micrograph showing planar view of Greek-cross Hall sensor device, (c) measured carrier mobility and sheet density, as a function of temperature, and (d) sheet resistance as a function of temperature.

a multifunctionality Hall sensor monitoring both current and temperature. The frequency bandwidth of the AlN/GaN Hall sensor, determined by the device rise time, is measured at 9.8 MHz. We also report on the observations of a phase shift between the measured Hall signal and applied magnetic field that has potential as a novel method to monitor line current and to eliminate the Hall offset.

II. Growth and Fabrication of AlN/GaN Micro-Hall Sensors by MBE

To realize Hall effect sensors at high frequency and high temperature, we utilized AlN/GaN high-electron-mobility transistor (HEMT) structures. The heterostructures were grown using a nitrogen plasma-assisted Veeco Gen II molecular beam epitaxy (MBE) system. The HEMT structures consisted of a 1.5-μm GaN buffer, a 3.5-nm AlN barrier, and a 1.5-nm GaN cap layer [Fig. 1(a)], which were deposited on top of a sapphire substrate having hydride vapor phase epitaxy (HVPE) grown 5-μm-thick, Fe-doped, semi-insulating (SI), GaN template.

During the growth of the epitaxial heterostructure, the substrate temperature was kept at 796 °C. Active nitrogen was supplied by radio frequency plasma with power maintained at 350 W and a flow rate of 0.50 sccm, which corresponded to a 0.25-mL/s deposition rate. For the growth, the flux of Ga/N ratio is greater than 1; during AlN deposition, the "Ga" shutter was always kept open to enhance "Al" atom diffusion kinetics to achieve a smooth surface morphology. After completion of the growth process, the excess "Ga" metal droplets present at the sample surface were removed by rinsing in HCl bath for approximately 20 min. The interface and structure quality of the as-grown HEMT heterostructure were investigated by using high-resolution X-ray diffraction (HR-XRD). To process the Greek-cross Hall effect sensor devices, we employed a Cl-based inductively coupled plasma (ICP) dry etch. Ohmic contacts were formed by depositing a Ti (25 nm)/Al (100 nm)/Ni (50 nm)/Au (150 nm) multilayer metal stack, followed by rapid thermal annealing (RTA) at 800 °C for 30 s, in 5-sccm flow of N_2 atmosphere. A planar image of the fabricated Greek-cross Hall effect sensor device is shown in Fig. 1(b). The fabricated Hall effect sensors were mounted on a nonmagnetic chip carrier and wire bonded. The frequency response experiments on the Hall effect sensor were conducted using a pulsed voltage bias via wave generator (Rigol DG2041A) at 0.5-V peak voltage with a rise time of 5 ns. The preamplified (SRS model SR560 low-noise preamplifier) output Hall voltage with respect to applied magnetic field was monitored using a digital oscilloscope (Rigol DS1202Z-E).

III. Behavior of the AlN/GaN Micro-Hall Sensor

After fabrication of the Greek-cross Hall effect sensor, the output voltage of the sensor was investigated. The measured voltage from contacts C_1 to C_2 in Fig. 1(b) consists of the magnetic field-induced Hall voltage V_H and an added offset voltage α due to the difference in contact resistance, geometrical asymmetries, and thermal gradients from contacts C_3 to C_1 and C_3 to C_2; the output signal of the Hall effect sensor can be described as [9]

$$V_{\text{out}} = G_H \frac{r_H}{q N_{2\text{DEG}}} I_b B_\perp + \alpha \tag{1}$$

where G_H is the device geometrical factor, and r_H represents the influence of material-based scattering factor, which is approximated to ($r_H = 1$), I_b is the Hall effect sensor bias current from contacts C_3 to C_4, $B_\perp$ is the applied magnetic field, α is the Hall offset, q is the elemental charge, and $N_{2\text{DEG}}$ is the sheet carrier density of the 2DEG at the AlN/GaN interface. Note that when Hall offset $\alpha = 0$, (1) defines only the Hall voltage (V_H) of Hall effect sensor. In our previous report [10], we introduced a new method to remove the offset voltage. The bias current of Hall effect sensor can be represented as

$$I_b = v_d A q \left(\frac{N_{2\text{DEG}}}{t} \right) \tag{2}$$

where $v_d = \mu \text{E}$ is the carrier velocity, μ is the charge carrier mobility, E is the applied electric field, A is the cross-sectional area, and t is the effective thickness of the current carrying channel. These parameters can be found from Hall measurements of the carrier mobility, sheet density, and sheet resistance measured for the as-grown AlN/GaN heterostructures. For example, for the AlN/GaN heterostructure, Fig. 1(c) gives the electron mobility and sheet density measured on the Greek-cross Hall effect sensor structure across a wide temperature range. The 2DEG electron mobility can depend on electron scattering events due to many sources, such as, dislocations, deformation potential, piezoelectric potential, optical phonon, ionized impurities, and interface roughness at the heterostructure interface [11], [12]. For the temperature range of −73 °C to 407 °C, the 2DEG mobility as a function of temperature for the AlN/GaN heterostructure in Fig. 1(c) follows a $\mu = AT^{-1.54}$ power law. This indicates that optical phonon scattering plays the dominant role in mobility as a function of temperature [13], [14]. Meanwhile,

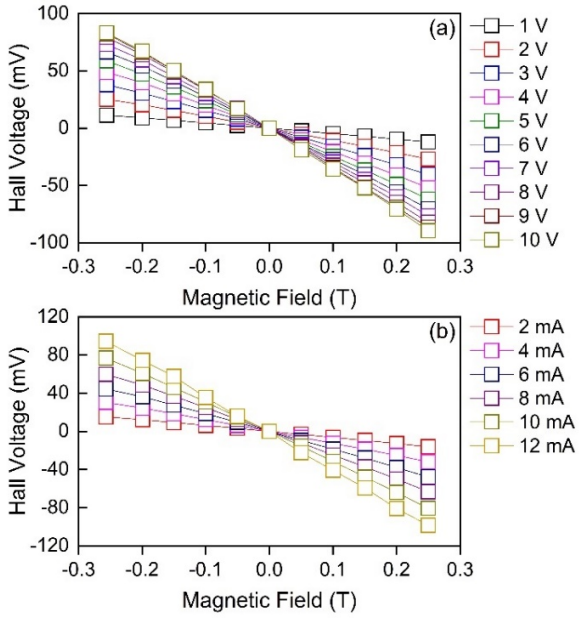

Fig. 2. Measured Hall voltage as a function of magnetic field operated under (a) constant voltage and (b) constant current bias mode for the AlN/GaN micro-Hall sensor at RT.

the observed change in electron mobility below −73 °C is also expected and reflects the transition to the deformation potential playing the dominant role on the mobility behavior [12]. Likewise, Fig. 1(d) shows the measured sheet resistance of the AlN/GaN Hall sensor linearly increasing with temperature over a range of 30 °C–380 °C, with the temperature coefficient of 9200 ppm/°C, which enables multifunctionality to Hall sensor, such as both current and temperature sensing application in a single chip.

IV. Comparison Between the AlN/GaN and $Al_{0.2}Ga_{0.8}N$/GaN Micro-Hall Sensors

To put the performance of the AlN/GaN Hall effect sensor in perspective, we compare it to a similarly constructed (cap) 5-nm GaN/20-nm $Al_{0.20}Ga_{0.80}N$/1.5-μm GaN/3.5-μm SI GaN (HVPE)/c-sapphire Hall sensor [15]. For a practical Hall sensor, the Hall voltage versus magnetic field relationship and sensitivity must remain linear over a wide range of magnetic field strength.

The AlN/GaN Hall sensor response follows a linear relationship with magnetic field [Fig. 2(a)], while the sensor is biased with a supply voltage of 1–10 V and magnetic field strength sweeping from −0.25 to 0.25 T. Similarly, the Hall voltage versus applied bias current from 1 to 12 mA also follows a linear response [Fig. 2(b)] with magnetic field.

To have a better understanding of the AlN/GaN Hall effect sensor specifications, the performance of the sensor can be quantified by calculating absolute sensitivity (S_a), supply-voltage related-sensitivity (S_{svrs}), and supply-current-related sensitivity (S_{scrs}). The Hall sensitivity is often estimated by using the expression [15]

$$S_a = \frac{dV_H}{dB_\perp}. \tag{3}$$

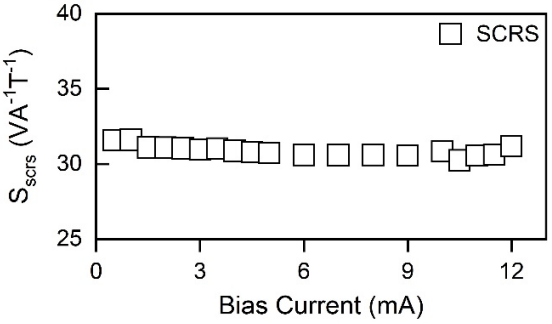

Fig. 3. Calculated "S_{scrs}" as a function of bias current for AlN/GaN Hall sensor. Maximum standard deviation of data points is ±1%.

However, the sensitivity depends directly on the bias voltage and current. For this reason, S_{svrs} is calculated as S_a divided by the bias voltage V_b and expressed as

$$S_{\text{svrs}} = \frac{1}{V_b}\frac{dV_H}{dB_\perp} \tag{4}$$

which implies that

$$S_{\text{svrs}} = \mu_H G_H \frac{r_H}{\left(\frac{L}{W}\right)}. \tag{5}$$

Similarly, one can also define the bias current-related sensitivity as

$$S_{\text{scrs}} = \frac{1}{I_b}\frac{dV_H}{dB_\perp} \tag{6}$$

which implies that

$$S_{\text{scrs}} \approx \frac{1}{qN_{2\text{DEG}}}. \tag{7}$$

For example, Fig. 3 gives the sensitivity S_{scrs} as a function of bias current I_b. It is evident that S_{scrs} for the AlN/GaN Hall sensor is almost constant to 1.1% for a wide range of bias current at room temperature (RT).

From (7), S_{scrs} is inversely dependent on the 2DEG sheet carrier density and is stable as a function of bias current. This indicates that carrier fluctuations in the AlN/GaN 2DEG, such as those caused by thermal or electrical activation of traps, are negligible at RT. To put these results in perspective, Fig. 4(a) demonstrates that under voltage bias, AlN/GaN shows superior performance compared to a similarly fabricated $Al_{0.2}Ga_{0.8}N$/GaN Hall effect sensor. This result is due to a lower sheet resistance along the 2DEG formed at the AlN/GaN interface, and hence, for a given voltage bias, the sensor drives more current through the 2DEG AlN/GaN interface relative to the higher sheet resistance for the $Al_{0.2}Ga_{0.8}N$/GaN heterostructure Hall sensor (350 Ω/sq) [15], [16]. From (5), when the Hall sensor is under voltage bias, the output Hall signal is directly proportional to the electron mobility. However, this points more generally to a difficulty in comparing Hall sensors. Two AlN/GaN sensors, operating under the same bias current, may be operating under a very different applied voltages and are not equivalent. Perhaps for better comparison, the Hall sensor performance should be measured in terms of applied

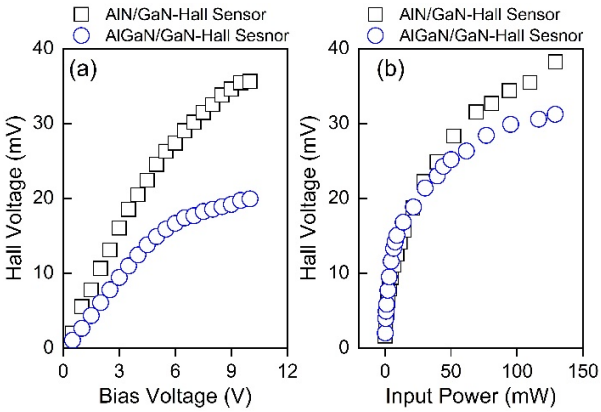

Fig. 4. Hall voltage for AlN/GaN and $Al_{0.2}Ga_{0.8}N$/GaN Hall sensors as a function of (a) voltage bias and (b) input power for a fixed magnetic field of 0.1 T at RT. Maximum SD of data points is ±4.2%.

power at the same current. The output Hall voltage in terms of dissipated power (P) can described as [17]

$$V_H = \mu_H G_H \frac{r_H}{\frac{L}{W}} V_B B_\perp \tag{8}$$

$$V_H = G_H r_H P^{\frac{1}{2}} \left[\frac{\mu_H}{N_{2\text{DEG}} q}\right]^{\frac{1}{2}} \left[\frac{W}{L}\right]^{\frac{1}{2}} B_\perp \tag{9}$$

then

$$P = \frac{V_H^2 N_{2\text{DEG}} q}{G_H^2 r_H^2 \mu_H B_\perp^2} \left[\frac{L}{W}\right] \tag{10}$$

where V_H is the Hall voltage, $N_{2\text{DEG}}$ is the 2DEG sheet carrier density, μ_H is the Hall mobility of the electrons, and L/W is the length-to-width ratio of the device conductive channel. Fig. 4(b) shows the measured power-dependent Hall response of both the AlN/GaN and $Al_{0.2}Ga_{0.8}N$/GaN micro-Hall sensors. Results demonstrate that above ∼40-mW input power, the AlN/GaN sensor output is a superior Hall sensor. The supply power-related sensitivity (SPRS) for the AlN/GaN sensor is ∼1.4 $VW^{-1}T^{-1}$, and for the $Al_{0.2}Ga_{0.8}N$/GaN sensor, it is ∼0.9 $VW^{-1}T^{-1}$ above 40 mW of power supply. However, at power levels below 40 mW, the performance of the $Al_{0.2}Ga_{0.8}N$/GaN Hall sensor appears slightly better.

V. AlN/GaN Hall Sensor Temperature Dependence

The AlN/GaN Hall sensor is designed to operate within circuits at extreme high temperatures and for harsh environmental applications; therefore, it is necessary to check Hall sensor temperature stability and performance. To understand the effects of thermal load on the AlN/GaN Hall sensor, we have performed temperature-dependent Hall measurements on the fabricated devices in a closed cryostat. Fig. 5(a) and (b) shows the response of the Hall effect sensor as a function of temperature subjected to bias with constant voltage or constant current, respectively.

For practical applications, it is desired that the output voltage of the sensor should show a linear response to magnetic field over a wide range of temperature. The AlN/GaN device exhibits a linear response to magnetic fields in the range of −0.25 to 0.25 T throughout the temperature range

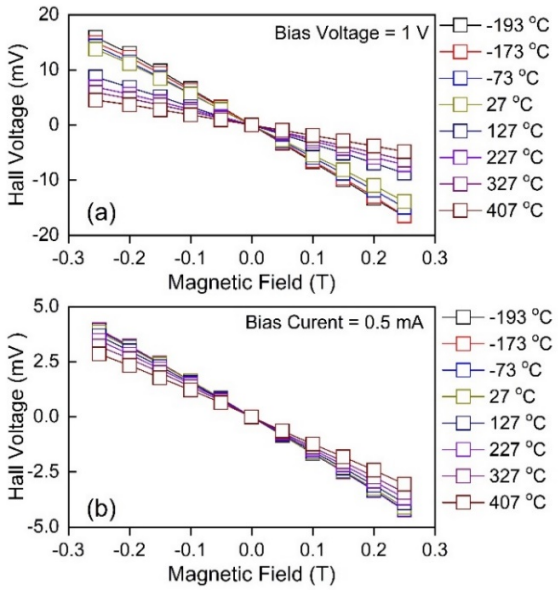

Fig. 5. Hall voltage versus magnetic field in the range of −0.25 to 0.25 T, in the AlN/GaN Hall sensor, over a wide range of temperature under (a) 1.0-V constant voltage bias and (b) 0.5-mA constant current bias.

of −193 °C to 407 °C. Overall, the AlN/GaN sensor output Hall voltage showed relatively stable performance over the wide temperature range, while the device was operated in the constant current mode. The temperature-dependent absolute sensitivity (S_a) for these AlN/GaN micro-Hall devices was found to be 64, 55, and 19 mV/T at −196 °C, RT, and 407 °C, respectively, for constant 1-V bias. Similarly, for 0.5-mA constant bias current, the absolute sensitivity (S_a) for these AlN/GaN micro-Hall devices was found to be 16.4, 16, and 12.5 mV/T at −196 °C, RT, and 407 °C, respectively. However, low-temperature tests are also important to explore the capability of Hall effect sensor in space atmosphere, for example, the temperature on Mars can be as high as 20 °C and as low as about −153 °C. Two better ways to quantify the temperature-dependent Hall effect sensor efficiency, such as supply voltage-related sensitivity S_svrs (T) and supply current-related sensitivity S_scrs (T), are calculated using (4) and (6) and shown in Fig. 6(a) and (b), respectively. For the AlN/GaN Hall sensor, S_svrs values (T) are estimated to be 0.064, 0.055, and 0.019 T^{-1}, and similarly, S_scrs (T) values are calculated to be 32.8, 32, and 25 $VA^{-1}T^{-1}$ at −193 °C, RT, and 407 °C, respectively. The observed slight decreasing trend in S_scrs (T) and the prominent change in S_svrs (T) as a function of temperature indicate a change in the sheet density due to ionized impurities and/or a drop in the drift velocity caused by phonon scattering at higher temperature. From (5), S_svrs is directly proportional to mobility, which exhibits a substantial ∼87% change over the temperature range [Fig. 1(c)]. From (7), S_scrs is inversely proportional to the sheet density, which only decreased by ∼18% over the temperature range and therefore supports a relatively stable S_scrs (T). The results indicate that the constant current mode is the preferred mode of operation for high-temperature applications.

Another important physical parameter that describes the Hall effect sensor performance with reference to temperature

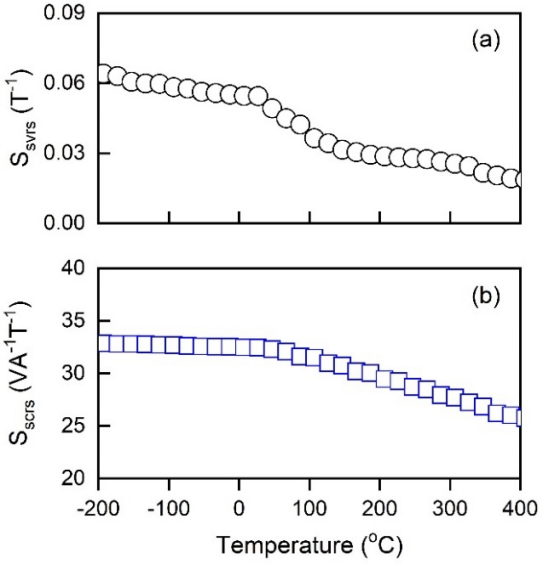

Fig. 6. Calculated (a) SVRS with a maximum standard deviation of the data points is ±5.9% and (b) SCRS as a function of temperature for AlN/GaN micro-Hall sensors (maximum SD of data points is ±1%).

is the temperature coefficient of the magnetic sensitivity, T_{CMS}. Heteroepitaxial grown AlN/GaN Hall sensor structures can potentially undergo strain relaxation due to high operating temperatures. To quantify the temperature stability of the AlN/GaN Hall sensor, we calculated the T_{CMS} by fitting to S_{scrs} (T) data across the tested temperature range using the expression

$$T_{CMS} = \frac{1}{S_{scrs}(T_0)} \times \frac{\Delta(S_{scrs}(T))}{\Delta T} \tag{11}$$

where $S_{scrs}(T_0)$ refers to the data acquired at the lowest experimental temperature. The obtained temperature coefficient of magnetic sensitivity for the AlN/GaN Hall sensors is ∼557 ppm/°C up to 407 °C. This value is in between previously reported AlGaN/GaN values that range from 103 to 1000 ppm/°C and Si (800 ppm/°C, for temperature range −10 °C to 130 °C) Hall sensors, respectively [3], [5], [15], [18]. The T_{CMS} comparison discrepancy arises between the Hall sensor due to the measurement taken at different temperature ranges and activation of defect density, trap states, unintentional doping, and contact nature. Therefore, very stable sheet carrier density plays an important role in achieving low T_{CMS} of the Hall effect sensor. This result shows that the AlN/GaN Hall sensor has potential high-temperature stability over the measured range of −193 °C to 407 °C, respectively, which is promising for high-temperature harsh environment applications. A benchmark of the fabricated AlN/GaN Hall sensor is presented in Table I, comparing it to a previously reported state-of-the-art Hall sensor [3], [4], [15], [19], [20], [21].

VI. Frequency Response of AlN/GaN Hall Sensor

Recent advancements in III-nitride and SiC high-power devices enable operation in the megahertz regime. As a result, Hall sensors designed to monitor high-power devices must also be capable of monitoring the produced high-frequency magnetic fields to sense potential catastrophic changes. To investigate the frequency response of the Hall sensor, we performed frequency-dependent Hall measurements. The rise time of Hall sensor output voltage was estimated by using the following expression:

$$V(t) = V_o\left(1-e^{-t/\tau}\right) \tag{12}$$

where V_o is the initial voltage and $V(t)$ is the voltage at time t. The rise time, $\tau(= RC)$, is the time taken to raise the voltage across the components from 0% to 63.2%, i.e., $(1-e^{-1})$ of its final value.

The data presented in Fig. 7 allow a comparison of the Hall offset rise time and sheet resistance of the AlN/GaN Hall sensor. It is evident from Fig. 7 that the Hall offset rise time of the AlN/GaN sensor increases with temperature. A similar trend is observed for the sheet resistance and Hall-offset voltage change with respect to temperature. This phenomenon of increase in sheet resistance with temperature is likely due to decrease in carrier velocity, which highlights the importance of low sheet resistance in Hall sensors designed for high-frequency applications. Fig. 8 shows the output Hall voltage obtained in response to a magnetic field of (−) 60 mT, with an input bias of 0.5-V peak voltage at 50-kHz square wave,

TABLE I
Benchmarking of AlN/GaN Micro-Hall Sensor With Previously Reported State-of-the-Art Hall Sensor

Materials	Temperature (°C)	S_{svrs} at 25 °C (T^{-1})	S_{scrs} at 25 °C ($VA^{-1}T^{-1}$)	T_{CMS} (ppm/°C)	Frequency range
Si [3]	-10 - 130	0.067	40-86	800	~1 MHz*
$In_{0.52}Al_{0.48}As/In_{0.8}Ga_{0.2}As$ [19]	-17 - 40	0.98	320	1.28	1 KHz
$Al_{0.12}In_{0.88}Sb/InSb$ [20]	-196 - 30	0.36	1220	n/a	20 KHz
$InAs/Al_{0.2}Ga_{0.8}Sb$ [4]	-100 - 150	0.2-0.9	65-302	5780	n/a
AlGaAs/InGaAs/GaAs [21]	-100 - 180	0.25	20-100	800	≤ 1 KHz*
AlGaN/GaN [15]	-183 - 252	0.013	113	1000	3 MHz**
AlN/GaN (present work)	-193 - 407	0.055	32	553	9.8 MHz

* With uncertainty, ** To be published

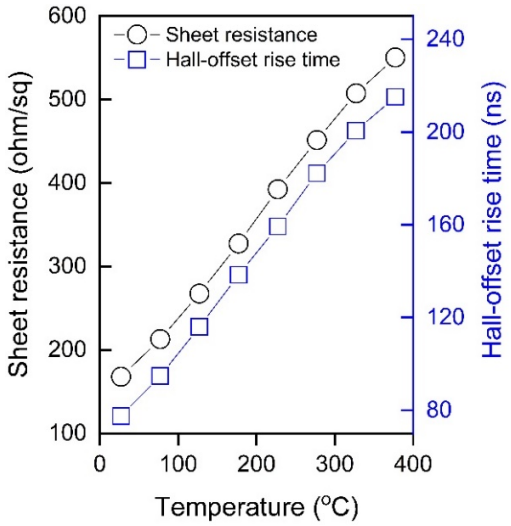

Fig. 7. Comparison of sheet resistance and Hall offset rise time for 50-kHz square bias signal of 0.5-V peak as a function of temperature; in the AlN/GaN Hall sensor, the maximum standard deviation data are ±3.2%.

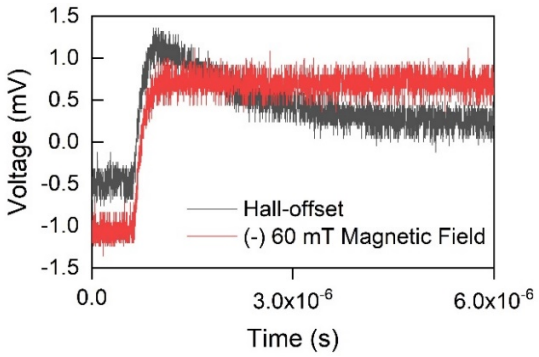

Fig. 8. Hall-offset and Hall voltage signal obtained at RT for 50-kHz square wave of 0.5-V peak bias signal in the AlN/GaN Hall sensor.

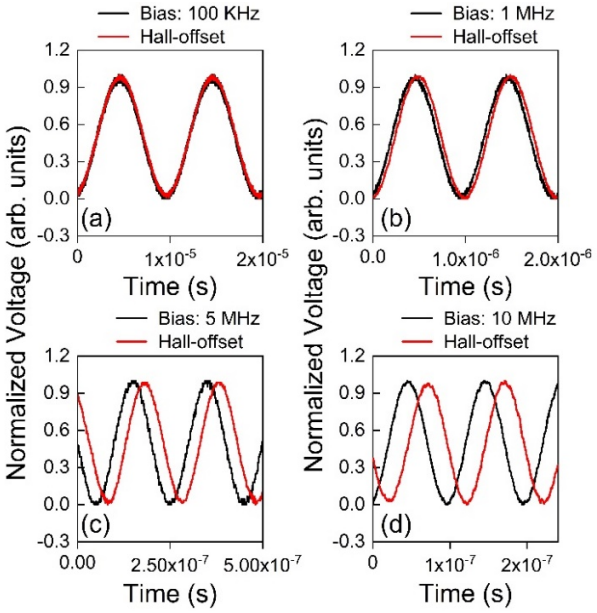

Fig. 9. Phase response of Hall offset in the AlN/GaN micro-Hall sensor measured at RT on various frequencies of applied bias (0.5-V peak voltage).

applied to the Hall sensor using a waveform generator (Rigol DS 1202Z-E).

Also, the rise time (τ) of Hall voltage for AlN/GaN Greek-cross Hall sensor is determined by using (12). The calculated rise time is ~102 ns for an applied magnetic field of (−) 60 mT. The frequency bandwidth of this AlN/GaN Hall sensor is approximately 9.8 MHz, determined by taking the inverse of the rise time. Furthermore, to investigate the phase shift correspondence between the Hall output signal and bias frequency, we conducted systematic frequency-dependent Hall measurements on the AlN/GaN Hall effect sensor. The main goal was to investigate the response of AlN/GaN Hall effect sensor as a function of frequency. This study was carried out in two steps as follows: 1) observing the Hall-offset response by varying the frequency of input bias voltage and 2) examining the output Hall voltage response with respect to the magnetic field as well as the frequency of input bias voltage. Fig. 9 illustrates the phase shift in Hall offset in the AlN/GaN Hall sensor as a function of the frequency of voltage bias (without an output amplification circuit, the sensor output directly connected to oscilloscope). Meanwhile, the output sine

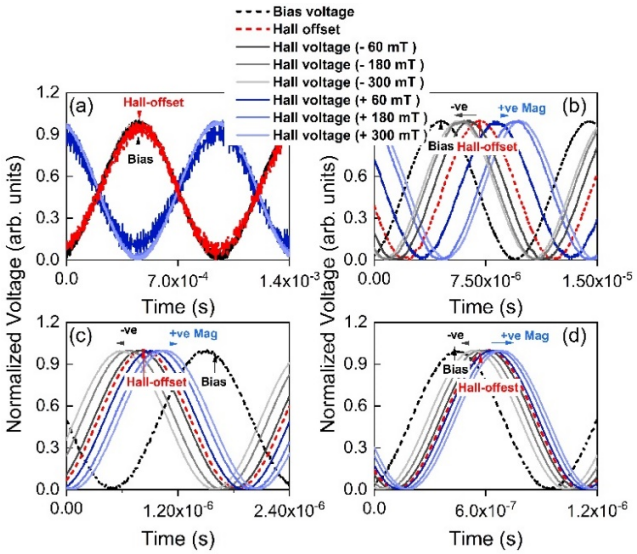

Fig. 10. Representative phase response of Hall voltage and Hall offset in the AlN/GaN micro-Hall sensor with respect to the frequency: (a) 1 KHz, (b) 100 KHz, (c) 500 KHz, and (d) 1 MHz of voltage bias (0.5-V peak voltage), respective data captured at RT (sensor output voltage is captured using a signal amplification readout circuit).

waveform of Hall offset is comparable to the reference bias signal without any distortion in waveform, which demonstrates that the Hall sensor can operate up to 10 MHz and also reveals that the Hall offset shows a phase shift as the frequency of voltage bias increases. The observed phase shift as a function of applied frequency of bias vintage can be attributed to the time constant (τ) of Hall effect sensor. Furthermore, to compare the phase shift between Hall offset and Hall voltage for AlN/GaN micro-Hall sensor, we recorded the Hall voltage phase shift as a function of the frequency of voltage bias and the applied magnetic field, and the corresponding data is shown in Fig. 10. There is a noticeable phase shift observed in Hall voltage relative to Hall offset with the influence of applied magnetic field.

As expected, we observed an opposite direction of phase shift in the Hall voltage relative to the Hall offset while changing the direction of applied magnetic field, as shown in Figs. 10 and 11.

The observed phase shift in Hall voltage with applied magnetic field is mainly due to change in Hall-electric potential across the Hall measurement contact terminals. Alternatively, we can refer this to the change in time constant, $\tau(= RC)$, of the Hall effect sensor. The Hall sensor resistance (R) and capacitance (C) across the Hall voltage measurement terminals C1 and C2 [as shown in Fig. 1(b)] can be described as $R = \rho L/A$ and $C = \kappa A/d$, where ρ is the resistivity, κ is the dielectric constant of the medium between the capacitor plates, A is the area of capacitor plates, and d is the separation between the capacitor plates. Here, the capacitance across the Hall voltage measurement contacts C1 and C2 can be treated as a conductive parallel plate capacitor, where Hall voltage generated by magnetic field is equivalent to charging a capacitor. According to the standard capacitance equation, $C = q/V$, where q is the charge held across the contacts C1 and C2 and V represents the developed electric potential. Therefore, the capacitance due to Hall voltage across the

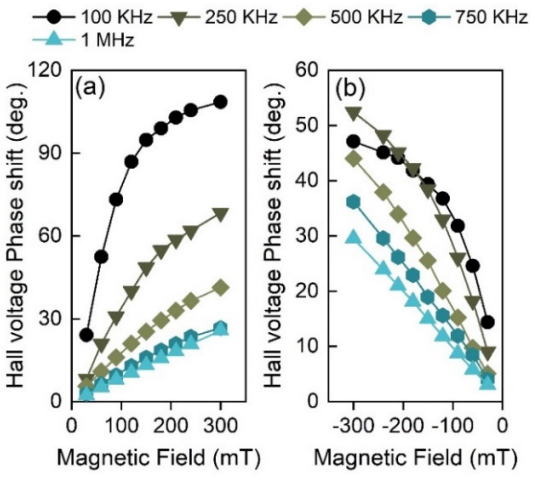

Fig. 11. Phase shift of the output Hall voltage in the AlN/GaN micro-Hall sensor as a function of applied magnetic fields (a) 0–300 and (b) −300–0 mT, measured for various frequencies of voltage bias (0.5-V peak voltage). Hall measurements were performed at RT and maximum standard deviation of data points is ±2.9%.

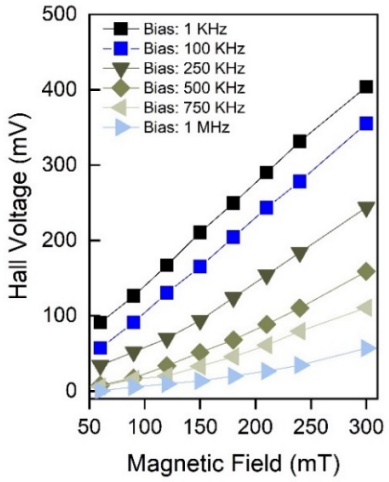

Fig. 12. Absolute amplitude output Hall voltage in the AlN/GaN micro-Hall sensor, obtained for various frequencies of voltage bias (0.5-V peak) and magnetic field at RT, and maximum standard deviation of data points is ±3%.

contacts C1 and C2 remains constant. However, the residual Hall offset voltage across these contacts is added to the Hall voltage for negative magnetic field and subtracted for positive applied magnetic field. The observed phase shift with applied magnetic field strength is directly related to the amount of Hall-electric potential that is added or subtracted from the Hall offset potential. This interpretation worked perfectly well, as evidenced by the data presented in Fig. 11(a) and (b). It clearly shows that the phase shift of the Hall voltage is directly correlated with the strength of the applied magnetic field.

Added to this, we also evaluated AlN/GaN micro-Hall sensor's Hall voltage as a function of magnetic field and frequency, as shown in Fig. 12. The gradual increase of output Hall voltage with the magnetic field can be understood by the expression in (1). Hall sensors have a wide range of applications; however, the current bottleneck for Hall effect sensors operating at high frequencies lies in the methodology of eliminating current-spinning Hall offset. Both the literature and current market research reveal that commercially available Hall sensors cannot exceed the frequency of ∼200 kHz due to limitations associated with the current-spinning circuit [6], [22].

Therefore, to address the high-frequency limitations of the current spinning technique, we propose the utilization of the magnetic field-induced phase shift in Hall voltage to enhance the application of current sensing Hall sensors at high frequency.

VII. Conclusion

In conclusion, we have grown AlN/GaN heterostructures by MBE and fabricated Hall effect magnetic field sensors. The AlN/GaN heterostructure was characterized as having a 2DEG sheet electron density of $\sim 2.15\times10^{13}/\text{cm}^2$, mobility of $\sim$1780 cm^2/Vs, and achieved a record low sheet resistance of ∼168 Ω/sq at RT. We have demonstrated the suitability of the AlN/GaN heterostructure for Hall sensor applications in terms of 1) sensitivity, 2) temperature stability, and 3) frequency response. It was observed that the AlN/GaN Hall sensor exhibits a supply voltage-related sensitivity (S_{svrs}) of $\sim 0.055\ \text{T}^{-1}$ and current-related sensitivity (S_{scrs}) of about $\sim 32\ \text{VA}^{-1}\text{T}^{-1}$, respectively. The supply power-related sensitivity (S_{sprs}) is 1.4 $\text{VW}^{-1}\text{T}^{-1}$ above 40 mW, which is higher than that of tested $Al_{0.2}Ga_{0.8}N$/GaN device. The AlN/GaN microscale Hall sensor exhibits high signal linearity under a wide range of current (∼0.2–12 mA) and voltage (∼0.5–10 V) biases for a significant range of applied magnetic field (50 mT–0.25 T) amplitudes. The sheet resistance of the AlN/GaN Hall sensor linearly increases with temperature over a range of 30 °C–380 °C, with a temperature coefficient of ∼9200 ppm/°C, which enables multifunctionality to Hall sensor, such as both current and temperature sensing application in a single chip. Importantly, our results demonstrate that above ∼40-mW input power, the AlN/GaN sensor output is a superior Hall sensor compared to similarly prepared $Al_{0.2}Ga_{0.8}N$/GaN. Furthermore, this study demonstrated the frequency response of the Hall effect sensor, while it was subjected to an ac bias mode. The frequency bandwidth of the AlN/GaN Hall sensor can be determined by inverse of the rise time and which is found to be ∼9.8 MHz. Meanwhile, the observed phase shift of Hall voltage relative to the applied magnetic field suggests the phase difference as a method to detect line current. Therefore, we proposed a method to detect ac line current by monitoring the phase shift of output Hall sensor signal. This work supports the integration of the AlN/GaN Hall effect material and device system into actual harsh environment industrial systems (e.g., electrified heavy-duty machines, motors, and trucks) for fault monitoring at high speeds.

References

[1] M. Chen and H. V. Poor, "High-frequency power electronics at the grid edge: A bottom-up approach toward the smart grid," *IEEE Electrific. Mag.*, vol. 8, no. 3, pp. 6–17, Sep. 2020, doi: 10.1109/MELE.2020.3005695.

[2] A. Hassan, A. Mahar, K. A. Faruque, S. Shetty, G. J. Salamo, and H. A. Mantooth, "A fast interface circuit using multiple signal paths for high bandwidth Hall sensors," in *Proc. 20th IEEE Interregional NEWCAS Conf. (NEWCAS)*, Jun. 2022, pp. 218–221, doi: 10.1109/NEWCAS52662.2022.9842177.

[3] G. S. Randhawa, "Monolithic integrated Hall devices in silicon circuits," *Microelectron. J.*, vol. 12, no. 6, pp. 24–29, Nov. 1981, doi: 10.1016/s0026-2692(81)80360-6.

[4] M. Behet, J. Bekaert, J. De Boeck, and G. Borghs, "InAs/$Al_{0.2}Ga_{0.8}$Sb quantum well Hall effect sensors," *Sens. Actuators A, Phys.*, vol. 81, nos. 1–3, pp. 13–17, Apr. 2000, doi: 10.1016/s0924-4247(99)00162-4.

[5] S. Koide, H. Takahashi, A. Abderrahmane, I. Shibasaki, and A. Sandhu, "High temperature Hall sensors using AlGaN/GaN HEMT structures," *J. Phys., Conf.*, vol. 352, Mar. 2012, Art. no. 012009, doi: 10.1088/1742-6596/352/1/012009.

[6] A. Bilotti, G. Monreal, and R. Vig, "Monolithic magnetic Hall sensor using dynamic quadrature offset cancellation," *IEEE J. Solid-State Circuits*, vol. 32, no. 6, pp. 829–836, Jun. 1997, doi: 10.1109/4.585275.

[7] D. Maier et al., "InAlN/GaN HEMTs for operation in the 1000 °C regime: A first experiment," *IEEE Electron Device Lett.*, vol. 33, no. 7, pp. 985–987, Jul. 2012, doi: 10.1109/LED.2012.2196972.

[8] J. Encomendero et al., "Room temperature microwave oscillations in GaN/AlN resonant tunneling diodes with peak current densities up to 220 kA/cm^2," *Appl. Phys. Lett.*, vol. 112, no. 10, pp. 1–5, Mar. 2018, doi: 10.1063/1.5016414.

[9] S. Shetty et al., "Thermal stability study of gallium nitride based magnetic field sensor," *J. Appl. Phys.*, vol. 134, no. 14, Oct. 2023, doi: 10.1063/5.0156013.

[10] G. J. S. Thomas P. White, S. Shetty, M. E. Ware, and H. A. Mantooth, "Micro-hall effect devices for simultaneous current and temperature measurements for both high and low temperature environments," U.S. Patent 11 137 310 B2, Oct. 5, 2021.

[11] L. Hsu and W. Walukiewicz, "Electron mobility in $Al_xGa_{1-x}N$/GaN heterostructures," *Phys. Rev. B, Condens. Matter*, vol. 56, no. 3, pp. 1520–1528, Jul. 1997, doi: 10.1103/physrevb.56.1520.

[12] M. N. Gurusinghe, S. K. Davidsson, and T. G. Andersson, "Two-dimensional electron mobility limitation mechanisms in $Al_xGa_{1-x}N$/GaN heterostructures," *Phys. Rev. B, Condens. Matter*, vol. 72, no. 4, pp. 1–11, Jul. 2005, doi: 10.1103/physrevb.72.045316.

[13] H. S. Alpert et al., "Sensitivity of 2DEG-based Hall-effect sensors at high temperatures," *Rev. Sci. Instrum.*, vol. 91, no. 2, Feb. 2020, Art. no. 025003, doi: 10.1063/1.5139911.

[14] A. Aminbeidokhti, S. Dimitrijev, J. Han, X. Chen, and X. Xu, "The power law of phonon-limited electron mobility in the 2-D electron gas of AlGaN/GaN heterostructure," *IEEE Trans. Electron Devices*, vol. 63, no. 5, pp. 2214–2218, May 2016, doi: 10.1109/TED.2016.2544920.

[15] T. P. White, S. Shetty, M. E. Ware, H. A. Mantooth, and G. J. Salamo, "AlGaN/GaN micro-Hall effect devices for simultaneous current and temperature measurements from line currents," *IEEE Sensors J.*, vol. 18, no. 7, pp. 2944–2951, Apr. 2018, doi: 10.1109/JSEN.2018.2794264.

[16] P. Sung Park, D. N. Nath, S. Krishnamoorthy, and S. Rajan, "Electron gas dimensionality engineering in AlGaN/GaN high electron mobility transistors using polarization," *Appl. Phys. Lett.*, vol. 100, no. 6, pp. 1–4, Feb. 2012, doi: 10.1063/1.3685483.

[17] M. A. Paun, J. M. Sallese, and M. Kayal, "Geometry influence on Hall effect devices performance," *UPB Sci. Bull. Ser. A*, vol. 72, no. 4, pp. 257–271, 2010.

[18] H. Lu, P. Sandvik, A. Vertiatchikh, J. Tucker, and A. Elasser, "High temperature Hall effect sensors based on AlGaN/GaN heterojunctions," *J. Appl. Phys.*, vol. 99, no. 11, Jun. 2006, doi: 10.1063/1.2201339.

[19] Y. Sugiyama, Y. Takeuchi, and M. Tacanot, "Highly-sensitive InGaAs-2DEG Hall device made of pseudomorphic $In_{0.52}A_{10.48}As/In_{0.8}Ga_{0.2}As$ heterostructure," *Sens. Actuators A, Phys.*, vol. 34, no. 2, pp. 131–136, Aug. 1992, doi: 10.1016/0924-4247(92)80184-5.

[20] V. P. Kunets et al., "Highly sensitive micro-Hall devices based on $Al_{0.12}In_{0.88}Sb$/InSb heterostructures," *J. Appl. Phys.*, vol. 98, no. 1, pp. 1–6, Jul. 2005, doi: 10.1063/1.1954867.

[21] N. Haned and M. Missous, "Nano-tesla magnetic field magnetometry using an InGaAs-AlGaAs-GaAs 2DEG Hall sensor," *Sens. Actuators, A Phys.*, vol. 102, no. 3, pp. 216–222, 2003.

[22] A. Lalwani et al., "Effect of geometry on the frequency limit of GaAs/AlGaAs 2-D electron gas (2DEG) Hall effect sensors," *IEEE Sensors Lett.*, vol. 7, no. 12, pp. 1–4, Dec. 2023, doi: 10.1109/lsens.2023.3320039.